Simulation and Experimental Validation of Microstructure Evolution of Sintered Ag Layer During Thermal Aging Using a Hybrid Potts-Phase Field Model

Xiao Hu
Delft University of Technology
Delft, The Netherlands
x.hu-1@tudelft.nl

Chao Gu
Fudan University
Shanghai, China
24110860040@m.fudan.edu.cn

Qiling Xing
Delft University of Technology
Delft, The Netherlands
qilingxing@tudelft.nl

René Poelma
Nexperia
Nijmegen, The Netherlands
rene.poelma@nexperia.com

Jianlin Huang
Ampleon
Nijmegen, The Netherlands
jianlin.hunag@ampleon.com

Hans van Rijckevorsel
Ampleon
Nijmegen, The Netherlands
hanvanrij60@gmail.com

Huib Scholten
Ampleon
Nijmegen, The Netherlands
huib.scholten@ampleon.com

Jiajie Fan
Fudan University
Shanghai, China
jiajie_fan@fudan.edu.cn

Marcel .H. Hermans
Delft University of Technology
Delft, The Netherlands
M.H.Hermans@tudelft.nl

Willem D. Van Driel
Delft University of Technology
Delft, The Netherlands
willem.van.driel@signify.com

Guoqi Zhang
Delft University of Technology
Delft, The Netherlands
G.Q.Zhang@tudelft.nl

2025 IEEE 75th Electronic Components and Technology Conference (ECTC) | 979-8-3315-3932-0/25/$31.00 ©2025 IEEE | DOI: 10.1109/ECTC51687.2025.00124

***Abstract*— The long-term reliability of sintered silver (Ag) layers in high-power electronics is strongly influenced by microstructural evolution during thermal aging. In this study, we present a hybrid Potts-Phase Field model that integrates discrete grain growth dynamics based on the Kinetic Mento Carlo method with continuous pore migration based on the Phase Field method to simulate the microstructure evolution of sintered Ag under high-temperature storage experiment. The model is written in Taichi Lang, a parallel language embedded in Python, to improve the efficiency and speed of large-scale microstructure simulation. The microstructural characterization results show that the sintered silver layer conforms to the normal grain growth characteristics and pore migration with increased aging time under air ambient at 200℃. The average grain size was fitted based on the grain growth kinetics model. The initial grain size of the experimental group was 0.31 μm, the grain growth index n was 2.04, and the grain growth rate K was 4.31×10^{-3}. The initial grain size of the simulation group was 0.29 μm, the grain growth index n was 2.71, and the grain growth rate K was 1.28×10^{-4}. The experimental and simulation results showed good consistency in the initial grain size and evolution trend, but there were certain deviations in the grain boundary migration rate and time scale mapping. This work provides a new tool for simulating richer coupling phenomena in the microstructure during the aging process of Ag sintering materials and points out the direction for subsequent model optimization and parameter calibration.**

Keywords*— Sintered Ag layer, Thermal Aging, Hybrid Potts-Phase Field Model, Grain Growth, Pore Migration, Microstructure Evolution

I. INTRODUCTION

Wide bandgap semiconductor devices, such as silicon carbide (SiC) and gallium nitride (GaN), have superior performance of high power density, high operating temperature, high switching frequency, and reduced energy consumption [1]. They are gradually replacing traditional silicon-based devices and are widely used in electric vehicles, renewable energy systems, 5G communications, data centers, aerospace, and high-end industries. This not only promotes the innovation of power electronics technology and the continuous upgrading of system integration but also puts higher requirements on the heat dissipation performance and long-term reliability of devices [2], [3].

Micro-nano metal particle sintering materials such as silver (Ag) sintering materials are widely used in power device packaging [2], [4]. These materials enable low-temperature sintering processes to produce interconnect layers with excellent electrical and thermal conductivity, meeting the strict operating requirements of high-power density devices in harsh environments. However, during long-term high-temperature and high-power operations, the microstructure of these sintered layers may undergo a series of changes. such as pore evolution and grain growth [5], [6]. Variations in grain size affect the electrical and thermal properties of materials by modulating electron-phonon scattering at grain boundaries while also influencing mechanical properties such as strength, hardness, plasticity, toughness, and fatigue behavior[7], [8]. At the same time, the evolution of pores is believed to cause local stress concentration, which may trigger structural failure, thereby destroying the long-term reliability of the device [9], [10]. Therefore, a comprehensive understanding of the mechanisms of grain growth, porosity evolution, and their interactions is essential for materials design and industry applications. This understanding paves the way for controlling microstructural evolution, optimizing the properties of sintered layers, and reliably predicting thermal aging behavior.

Advanced characterization techniques such as electron backscatter diffraction (EBSD) and transmission electron microscopy (TEM) can provide insights into microstructural observations. However, their high cost, demanding sample preparation, long time, or limited resolution make them inconvenient for comprehensive experimental prediction and assessment of long-term aging behavior. For simulation

2377-5726/25/$31.00 ©2025 IEEE
DOI 10.1109/ECTC51687.2025.00124

methods, at present, many simulation works focus on simulating macroscopic thermal and mechanical properties based on microstructures or simulating the sintering process and pore evolution process [9], [11], [12], [13]. There is still a lack of understanding of the synergistic effect of grain size and pores in the degradation mechanism of Ag sintering materials, and there is also a lack of simulation methods that can simultaneously simulate the co-evolution of porosity and grain structure on a long-term scale.

In this work, we introduced the hybrid Potts-Phase Field model. By discretizing the grain state through the Potts model and combining the Phase Field method to describe the continuous evolution of the component field, it is possible to simulate the coupled evolution process of grain growth and pore migration in the same framework and to capture the microstructural changes of the sintered silver layer under thermal aging. The paper is organized as follows: Section II details the experimental procedures and simulation methodology; Section III presents the experimental and simulated results along with discussion; and Section IV summarizes the conclusions and outlines directions for future work.

II. METHODOLOGY

A. Sintering and Thermal Aging Test Profiles

As shown in Fig.1, the Ag paste with a thickness of about 40 μm is first printed on a pure copper (Cu) substrate with Au/Pd coating, and a dummy Si chip with Au coating is placed to build a chip/sintered-Ag/substrate structure. Subsequently, the sample enters a high-temperature furnace for pressureless sintering according to the temperature-time curve, gradually heating up to 175°C and maintaining for 2 hours. After sintering, the sample was subjected to a high-temperature storage (HTS) experiment according to the JEDS22-A103 standard. It was stored in an air environment at 200°C for up to 1008 hours, and the samples were taken out for characterization at different time points such as 0 hours, 168 hours, 504 hours, and 1008 hours.

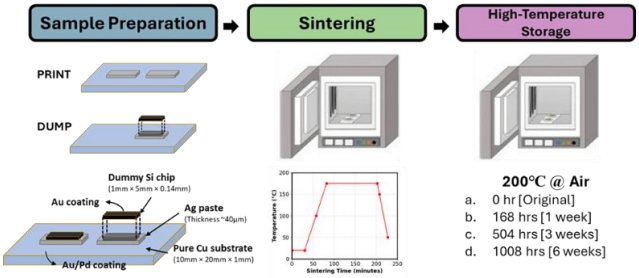

Fig. 1 Workflow of sintering process and High-Temperature Storage test.

B. Sample Preparation for EBSD Characterization

Since the sintered silver layer is a micron/nanoscale porous structure and very thin, the sample should be processed very carefully before EBSD characterization. The sample was cold-mounted at low temperature and low pressure. Then, it was mechanically ground and polished to show a flat surface. After polishing, the sample was cleaned using an ultrasonic cleaner. After that, argon ion milling was performed for 15 minutes with an ion beam current of 120 μA and a Gas Flow of 0.09 cm^3/min to reduce the damage to the surface caused by mechanical polishing. Before characterization, the sample surface was carbon-sprayed to avoid charging effects. Electron backscatter diffraction (EBSD) data and Focused Ion Beam-Scanning Electron Microscope (FIB-SEM) cross-sectional images were collected by the FEI Helios G4 system and processed by OIM 8.0 software and Image J.

C. Hybrid Potts-Phase Model Implementation

A hybrid Potts-phase field model is introduced here to simulate grain growth while tracking the subtle evolution of phase interfaces, which gives it unique advantages in studying complex multiphase microstructures and long-term dynamic processes [14]. The classical Potts model is usually used to simulate grain growth and recrystallization phenomena. The microstructure is discretized into a regular lattice grid, and each position represents a grain state, denoted as q_i, as shown in Fig. 2(a-b). Since multiple grain states can exist, the Potts model is also called the Q-state Potts model. When the number of states Q=2, the model is equivalent to the Ising model. The total system energy is expressed as

$$E_{Potts} = \sum J_{(q_i,q_j)}(1-\delta_{q_i,q_j}) \tag{1}$$

where the matrix $J(q_i, q_j)$ defines the interactive energy between neighboring grain states or pores states. Abnormal grain growth (AGG) can be simulated by modifying the interaction energy in matrix $J(q_i, q_j)$ to introduce preferential growth for certain grains. For normal grain growth (NGG), the matrix J should reflect uniform interaction energies between all grains.

In addition to the discrete phase states q_{ij}, each grid point also defines a composition field represented by a continuous order parameter $C_{ij}(x,t)$. The system evolution is governed by the Cahn-Hilliard equation:

$$\frac{\partial C}{\partial t} = M_C\left\{\nabla^2\frac{\partial E_v}{\partial C} - \kappa_C\nabla^4 C\right\} \tag{2}$$

where M_C is the mobility that controls the evolution speed and κ_C is the composition field gradient energy coefficient. E_v is the volume free energy. To describe the two-phase (in this case, Ag and pore) separation evolution process, as shown in Fig. 2(f), the form of E_v is

$$\begin{aligned} E_v\left(C_{ij},q_{ij}\right) = k\left[\left(C_{ij}-C_1\right)^2+\left(C_2-C_{ij}\right)^2\right] \\ +\alpha\left[\left(C_{ij}-C_3\right)^2 q_a+\left(C_4-C_{ij}\right)^2 q_b\right] \end{aligned} \tag{3}$$

The hybrid Potts-Phase Field model combines these two energy formulations, so the system's total energy is

$$E_{\text{hybrid}} = \sum_{i=1}^{N}\left(E_v\left(C_i,q_i\right)+\sum_{j=1}^{n}J\left(q_i,q_j\right)+\kappa_c\left(\nabla C_i\right)^2\right) \tag{4}$$

which allows simultaneous simulation of grain growth and composition field evolution.

In a Monte Carlo step (one Δt), a lattice point will be randomly selected, and its state will be tried to be changed, such as changing q=8 to q=9 in Fig. 2(c), and then the local energy

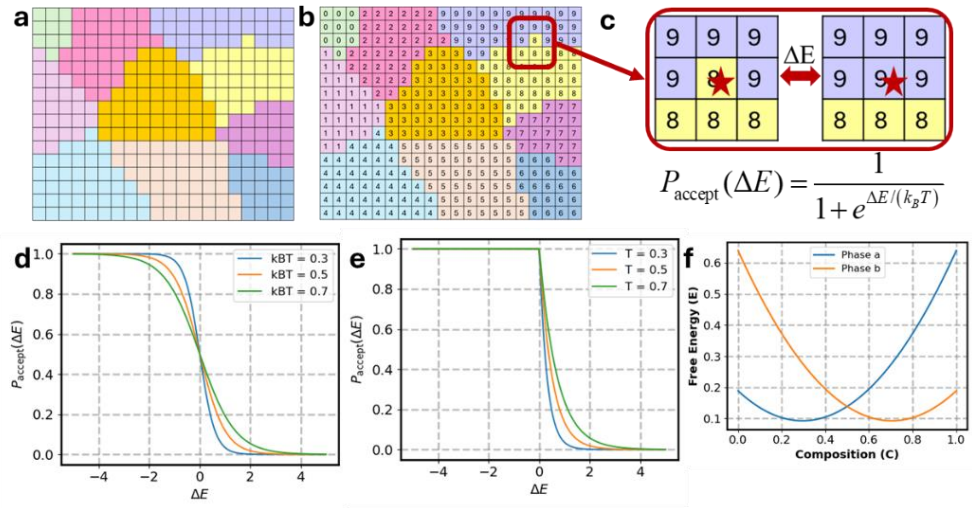

Fig. 2 Schematic diagram of lattice evolution in the hybrid Potts-Phase Field model, Monte Carlo update process, acceptance probability and phase free energy curves at different temperatures.

difference ΔE caused by this state change will be calculated, including the interaction energy difference in the Potts model and the free energy difference caused by the change of the component field in the phase field model. The calculation of the interaction energy considers the eight-neighbor relationship, and the evolution of the component field is updated using the explicit finite difference method according to the Cahn-Hilliard equation. Then, according to the Glauber dynamic probability Fig. 2(d) or Metropolis policy probability Fig. 2(e), it is decided whether to accept this change so that the system evolves towards a lower energy direction with probability P_{accept}, and the latest lattice state and component field distribution are recorded or displayed after the change. In the Glauber dynamics we used in this work, the probability of accepting an exchange is

$$P_{accept}(\Delta E) = \frac{1}{1+e^{\Delta E/(k_B T)}} \tag{5}$$

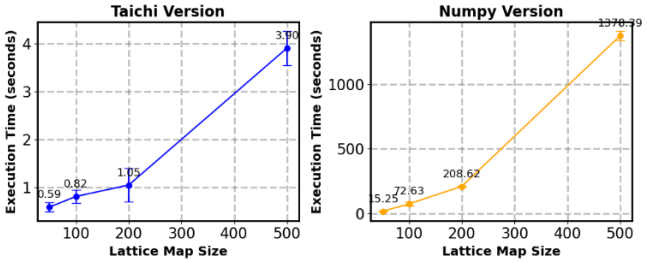

Fig. 3 Taichi vs. Numpy performance comparison: execution time for 100 Monte Carlo steps at different lattice map sizes

The hybrid model is implemented using the Q-state Potts Phase Field (QPPF) custom-made simulation package designed by the ECTM research group at Delft University of Technology. It uses the Taichi parallel language embedded in Python to improve the efficiency and speed of large-scale microstructure simulations [15]. Fig.3 shows the comparison between Taichi and Numpy's performance. It takes less than 4 seconds to perform 100 Monte Carlo steps on a 500×500 lattice map using an Intel Core i7-10610U CPU, while the Numpy version takes about 1300 seconds to perform the same operation.

III. Results and Discussion

A. Microstructure analysis from SEM and EBSD images

We conducted a high-temperature storage test in air at 200°C. A cross-sectional SEM image of the center of the sample was collected using FIB-SEM under 10 kV voltage, as shown in Fig. 4. It is obvious that the distribution of the pores at 0 hours is small and random. As the aging time increases, the pores gradually migrate and grow. Grain growth is also observed in the SEM image.

Fig. 5 shows the microstructure evolution of the sintered Ag layer under different aging times and the corresponding law of grain size change over time. Fig. 5 (a-d) are inverse pole figures that show the distribution diagram of grain orientation. As time passes, the grains grow and merge, and the pores migrate. Fig. 5(e) reflects the changing trend of grain size distribution and average grain size. As can be seen from the figure, with the increase of aging time, the grain size distribution moves toward the direction of large grains and gradually widens: in the early

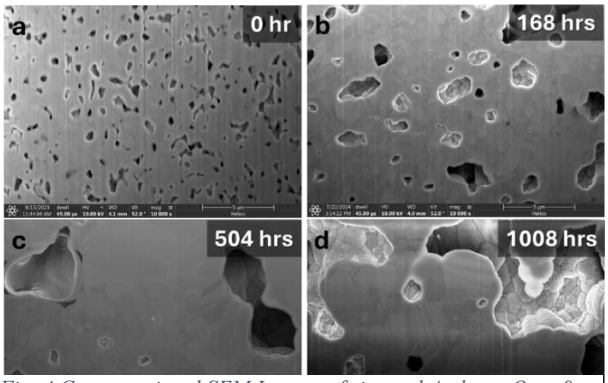

Fig. 4 Cross-sectional SEM Images of sintered Ag layer Over 0 to 1008 Hours in Air at 200°C.

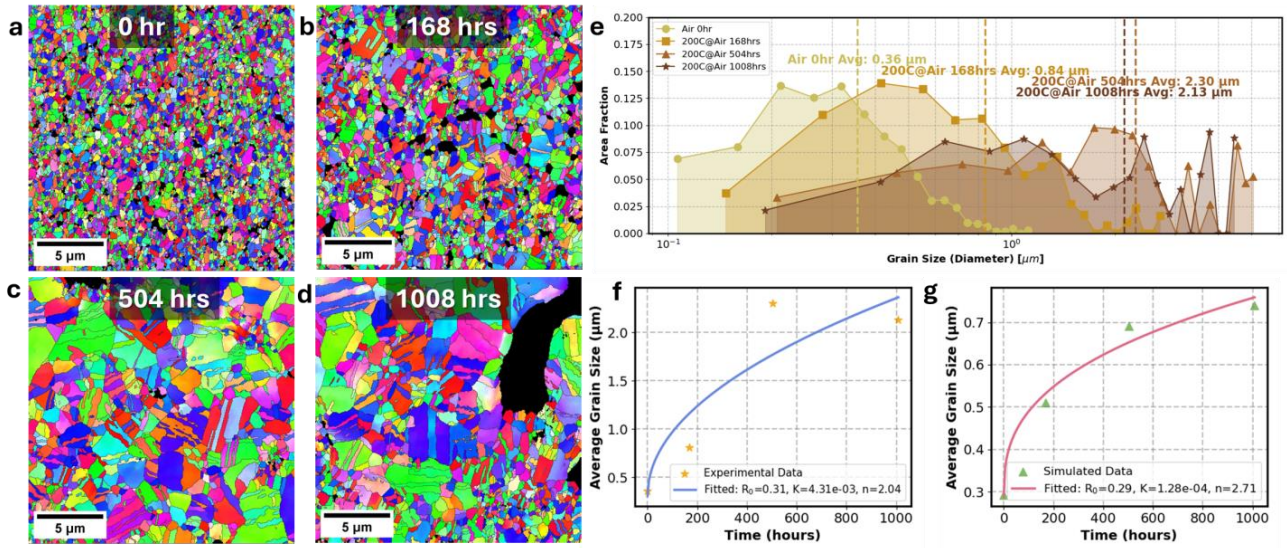

Fig. 5 (a-d) The distribution of grain orientation under different aging times; (e) Grain size distribution from IPF; Variation of average grain size with time in (f) experiments and (g) simulation results.

stage (such as 0 hours or 160 hours), the grain size distribution range is relatively concentrated, and the average grain size is small; while at a longer time (such as 500 hours or 1000 hours), the peak value of the distribution moves toward the direction of larger size, and the distribution range becomes wider, indicating that larger grains and smaller grains exist at the same time. The average grain size shows a monotonically increasing trend, and the growth rate slows down when the time is longer. There is no abnormally rapid growth of a few grains, and the grain distribution curve is in a single-peak form, consistent with the normal grain growth mode.

Here, we start with a simple parabolic grain growth model to summarize grain growth characteristics,

$$R^n - R_0^n = Kt \tag{6}$$

where R is the grain diameter, R_0 is the original grain diameter, K is the growth rate, and n is the growth exponent. Through experimental and characterization data, we obtained the grain growth index n to be 2.04 and the growth rate constant K to be 4.31×10^{-3}. The experimental results will be compared with the hybrid model results later.

B. Simulated Results

Fig. 6 shows the microstructural evolution of a 300-pixel * 300-pixel lattice map from 0 to 1000 KMC steps, including the evolution of grain growth (top row) and pore migration (bottom row). In this case, the number of Q is 8, q=0 represents the pore phase (Phase A, marked as Red), and q=1, 2, ..., 7 represents different grain orientation states of the Ag phase (Phase B, marked as Blue). The interaction energy J_{ij} between all states is set to 1. The k_BT in Eq. (5) defines the thermal energy scale of the system, which is set to 0.5. The settings of the parameters related to the volume free energy function are consistent with those in [14]. Periodic boundary conditions are used to define the boundary of the lattice map. The component evolution of Phase A and Phase B is controlled by the Cahn-Hillard equation and is considered to be conservative during the simulation. Therefore, the pores only migrate, while the different grain orientation states will change and grow, and small grains will merge into larger grains.

The lattice map is defined as 20 μm * 20 μm in actual size, and one Monte Carlo step is defined as one hour. Image J was used to extract the average grain sizes in the simulated lattice map at different time points, which were 0.29 μm, 0.51 μm, 0.69 μm, and 0.74 μm respectively. Substituting the results into the grain growth model, formula (5), we get the initial grain R_0 is 0.29 μm, the growth rate constant K is 1.28×10^{-4}, and the growth exponent n = 2.71.

Comparing Fig. 5(f) and (g), the overall trend of the experimental fitting curve is consistent with that of the simulation fitting curve. From a macroscopic point of view, the experiment and simulation may be controlled by similar dominant mechanisms. The experimental data show that n is 2.04, which is consistent with the classical parabolic growth model (n=2). In the simulation, n is 2.71, indicating that additional factors hinder the grain growth process, while the experimental growth rate is higher than the simulation, reflecting the insufficient grain boundary mobility in the simulation. The model has achieved good consistency in the initial grain size and macroscopic evolution trend, and further improvements are needed in terms of mobility parameter calibration and time scale mapping.

IV. Conclusion

In this study, we propose to use a hybrid Potts-Phase Field model to simulate the pore migration and grain growth of sintered Ag layers during thermal aging, and compare the characterization results of the microstructure of the Ag sintered layer during aging with the simulation results. The main findings are summarized as follows:

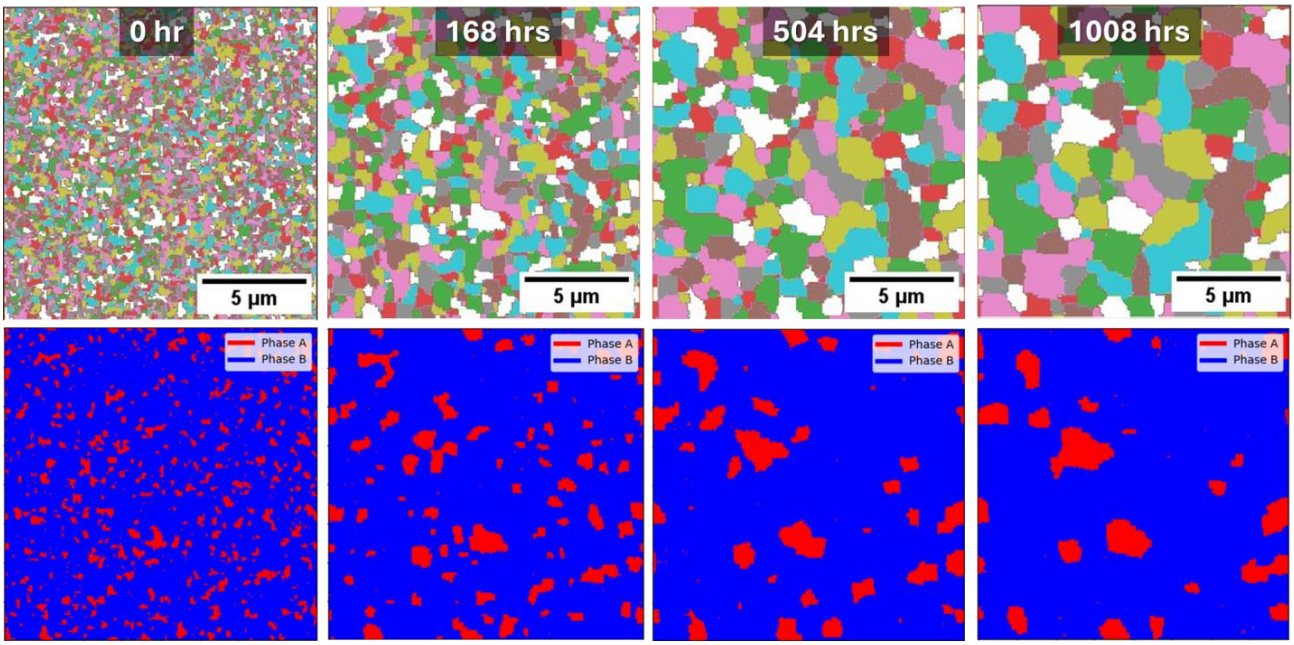

Fig. 6 Simulated Microstructure Evolution of Grain Growth (top row) and Pore aggregate (bottom row) from 0 to 1008 Hours.

- In the HTS test at 200°C under air ambient, grain growth and pore migration occur synchronously, and the grains show a normal grain growth mode. The experimental grain growth kinetics follows a parabolic growth model with the grain growth index n was 2.04, and the grain growth rate K was 4.31×10^{-3}.
- The hybrid model captures the coupled evolution of grain growth and pore migration at the same time. The simulation results show grain growth trends and pore migration patterns similar to the experimental results and also follow a parabolic growth model with a growth index of 2.71 and a growth rate of 1.28×10^{-4}.
- However, the growth rate of the simulated results is lower than that of the experimental results. Parameters such as grain boundary energy and component field mobility need to be further optimized and calibrated to improve simulation accuracy and predictive ability.
- The model is programmed using Taichi Lang embedded in Python to improve the efficiency and speed of large-scale microstructure simulation. It performs 100 Monte Carlo steps on a 500×500 lattice map using an Intel Core i7-10610U CPU in just 4 seconds.

The hybrid model in this study creates conditions for simulating richer coupling phenomena in the microstructure during the aging process of Ag sintering materials, which will help improve the reliability prediction and material design of high-power electronic products. Future work will focus on gradually calibrating the mobility parameters in the simulation model through more experiments to improve accuracy. In addition, extending the framework to include the exploration of evolution mechanisms under different aging conditions and considering the influence of multi-physics fields will further improve the predictive ability of the hybrid model.

ACKNOWLEDGMENT

This publication is part of the project called Fundamentals of Backside Metals System for 5G RF power Modules, which was financed by the Dutch Research Council (NWO) under project number 17969.

REFERENCES

[1] C. Buttay *et al.*, "State of the art of high temperature power electronics," *Materials Science and Engineering: B*, vol. 176, no. 4, pp. 283–288, Mar. 2011, doi: 10.1016/j.mseb.2010.10.003.

[2] A. A. Bajwa, Y. Qin, R. Reiner, R. Quay, and J. Wilde, "Assembly and Packaging Technologies for High-Temperature and High-Power GaN Devices," *IEEE Trans. Compon., Packag. Manufact. Technol.*, vol. 5, no. 10, pp. 1402–1416, Oct. 2015, doi: 10.1109/TCPMT.2015.2468595.

[3] J. G. Bai, J. N. Calata, and G. Lu, "Processing and Characterization of Nanosilver Pastes for Die-Attaching SiC Devices," *IEEE Transactions on Electronics Packaging Manufacturing*, vol. 30, no. 4, pp. 241–245, Oct. 2007, doi: 10.1109/TEPM.2007.906508.

[4] S. A. Paknejad and S. H. Mannan, "Review of silver nanoparticle based die attach materials for high power/temperature applications," *Microelectronics Reliability*, vol. 70, pp. 1–11, Mar. 2017, doi: 10.1016/j.microrel.2017.01.010.

[5] K. Mohan, N. Shahane, R. Liu, V. Smet, and A. Antoniou, "A Review of Nanoporous Metals in Interconnects," *JOM*, vol. 70, no. 10, pp. 2192–2204, Oct. 2018, doi: 10.1007/s11837-018-3081-z.

[6] S. Zhao, Y. Tong, C. Wang, and E. Yao, "Challenges and progress in packaging materials for power modules with high operation temperature: Review," *J Mater Sci: Mater Electron*, vol. 35, no. 35, p. 2237, Dec. 2024, doi: 10.1007/s10854-024-14002-4.

[7] P. Gadaud, V. Caccuri, D. Bertheau, J. Carr, and X. Milhet, "Ageing sintered silver: Relationship between tensile behavior, mechanical properties and the nanoporous structure evolution," *Materials Science and Engineering: A*, vol. 669, pp. 379–386, Jul. 2016, doi: 10.1016/j.msea.2016.05.108.

[8] C. C. Koch, *Nanostructured Materials: Processing, Properties and Applications*. William Andrew, 2006.

[9] K. Wakamoto, T. Otsuka, K. Nakahara, V. Mugilgeethan, R. Matsumoto, and T. Namazu, "Degradation Mechanism of Silver Sintering Die Attach Based on Thermal and Mechanical Reliability

Testing," *IEEE Transactions on Components, Packaging and Manufacturing Technology*, vol. 13, no. 2, pp. 197–210, Feb. 2023, doi: 10.1109/TCPMT.2023.3242423.

[10] D.-H. Li, W.-J. Xu, T.-Y. Liu, B. Zhang, Y. Liu, and Y.-H. Mei, "Influence of sintering process on high temperature cyclic deformation behavior and fatigue creep damage mechanism of sintered silver," *International Journal of Fatigue*, vol. 194, p. 108839, May 2025, doi: 10.1016/j.ijfatigue.2025.108839.

[11] X. Long, K. Chong, Y. Su, L. Du, and G. Zhang, "Connecting the macroscopic and mesoscopic properties of sintered silver nanoparticles by crystal plasticity finite element method," *Engineering Fracture Mechanics*, vol. 281, p. 109137, Mar. 2023, doi: 10.1016/j.engfracmech.2023.109137.

[12] Y. Su, G. Fu, C. Liu, C. Liu, and X. Long, "Fatigue crack evolution and effect analysis of Ag sintering die-attachment in SiC power devices under power cycling based on phase-field simulation," *Microelectronics Reliability*, vol. 126, p. 114244, Nov. 2021, doi: 10.1016/j.microrel.2021.114244.

[13] Y. Su *et al.*, "Thermo-elasto-plastic phase-field modelling of mechanical behaviours of sintered nano-silver with randomly distributed micro-pores," *Computer Methods in Applied Mechanics and Engineering*, vol. 378, p. 113729, May 2021, doi: 10.1016/j.cma.2021.113729.

[14] E. R. Homer, V. Tikare, and E. A. Holm, "Hybrid Potts-phase field model for coupled microstructural–compositional evolution," *Computational Materials Science*, vol. 69, pp. 414–423, Mar. 2013, doi: 10.1016/j.commatsci.2012.11.056.

[15] Y. Hu, T.-M. Li, L. Anderson, J. Ragan-Kelley, and F. Durand, "Taichi: a language for high-performance computation on spatially sparse data structures," *ACM Transactions on Graphics (TOG)*, vol. 38, no. 6, p. 201, 2019.